Electronic Supplementary Material (ESI) for Nanoscale.
This journal is © The Royal Society of Chemistry 2021

Shallow implanted SiC spin qubits used for sensing an internal spin bath and external YIG spins.

Jérôme Tribollet,[*,†] Dominique Muller,[‡] Stephane Roques,[‡] Jeremy Bartringer,[‡] and Thomas Fix[‡]

Institut de Chimie de Strasbourg, Universite de Strasbourg and CNRS, UMR 7177, 4 rue Blaise Pascal, CS 90032, F-67081 Strasbourg Cedex, France, and Laboratoire Icube, Universite de Strasbourg and CNRS, UMR 7357, 23 rue du Loess, BP 20, 67037 Strasbourg Cedex 2, France

E-mail: tribollet@unistra.fr

Supplementary Information

Details on the fabrication of shallow silicon vacancies.

First, we start with a high purity and semi-insulating commercial 4H-SiC wafer whose resistivity is $\geq 10^7\,\Omega\,cm$. There is no intentional Nitrogen doping in this HPSI 4H SiC wafer. Due to growth, this substrate already contains many bulk defects, including the silicon vacancies defects we are interested in here. As it is well known that those silicon vacancies spin qubits color centers can be removed by a high temperature annealing typically above $800^\circ C$, we started by a long $1100^\circ C$ thermal annealing under argon gaz of this wafer. As it is shown on Fig.2a, a cw EPR (electron paramagnetic resonance) study of this annealing process, called the Reset process, was performed

[*]To whom correspondence should be addressed
[†]Institut de Chimie
[‡]Laboratoire ICube

at room temperature under optical pumping. It is clearly seen on Fig.2a that after 8 days of such an annealing, the photo-EPR signal of V2 type silicon vacancies at X band (around 9.7 GHz) was no more detected. Using other reference pieces of this wafer, and using profilometry and ellipsometry experiments (not shown), we determined the oxidation rate of 4H-SiC by thermal oxidation under pure Oxygen at $1100\,^{\circ}C$, as well as the chemical etching rate of the resulting SiO_2 layer by a diluted solution of HF. In our experimental conditions, we found an etching rate close to 63 nm per minute, thus of roughly 1 nm per second. Of course, slower or faster etching rates of SiO_2 on SiC could be designed, depending on the HF solution concentration. Controlling the 4H-SiC oxidation rate and the SiO2 chemical etching rate, we fabricated a 74 nm oxide layer on our Reset and oxidized 4H-SiC wafer, which was then used as a sacrificial layer for the subsequent ion implantation process. Note that a sacrificial layer of SiO_2 could probably be coated directly on the SiC wafer, as a simpler alternative to our oxidation/etching process used here, but under the conditions that i/ the exact density and stoechiometry of the coated SiO_2 layer be known, otherwise it should be measured to adjust the energy of the C^+ ions implanted, and ii/ that the surface roughness of the SiO_2 coated layer is small compared to the precision required on the optimal implantation depth (target depth nearby the SiO_2 - SiC interface). Note that in our case, the RMS surface roughness of thermal oxide layer on SiC is $\Delta z_{SiO_2} \approx 0.2\,nm$, and that the SiC RMS surface roughness after HF etching of thermal oxide layer is $\Delta z_{SiC} \approx 0.7\,nm$ (as obtained by AFM, not shown here.) SRIM simulation indicated that for such a system, SiO_2 (74 nm)/4H-SiC(infinite), C^+ ions having an energy of around 23 keV would produce a maximum of silicon vacancies near the SiO_2/4H-SiC interface. Thus, 23 keV C^+ ions were implanted through this 74 nm oxide layer at a dose of $2\,10^{13}\,cm^{-2}$. The SiO2 was then removed from the implanted 4H-SiC sample by a full HF etching, producing a nearly half gaussian distribution of silicon vacancies below the SiC surface, with a maximum at the surface and a half width of around 25 nm, according to SRIM simulations (see further). Finally, as we wanted to activate a large enough ensemble of those shallow silicon vacancies created by ion implantation, we then performed a post implantation annealing of 90 minutes at $700\,^{\circ}C$ under argon gas, in order to optimize the amount of shallow silicon vacancies of V2 type in

this implanted 4H-SiC sample. Still using CW photo-EPR, we clearly observed the re-appearance of the silicon vacancies in our 4H-SiC sample as a result of this ion implantation process (see Fig.2b), as required for a full pulsed EPR study of their quantum spin coherence properties.

Fig.8 shows the result of a SRIM numerical simulation of the ion implantation process in 4H-SiC through a sacrificial SiO2 layer, used here to create shallow V2 spins.

The Fig.9 compares the V2 infrared photoluminescence spectrum of the 8 days annealed 4H-SiC reference sample and the one of the fully processed and ion implanted 4H-SiC sample studied here in details.

All the magnetic resonance experiments presented here were performed on a commercial ELEXYS E580 pulsed EPR spectrometer from BRUKER operating at X band (9.3 - 9.7 GHz). This pulsed EPR spectrometer was interfaced by means of an optical fiber to a standard external photoluminescence setup, allowing both laser light excitation at 785 nm and photoluminescence collection and detection, following previously published methodologies for fiber based OP-pulsed EPR, OP-PELDOR and ODMR.[4,7]

Details on the analysis of CPMG DD experiments on the shallow V2 spins.
Following the previously described method used for shallow NV centers in diamond,[10] we extracted $T_{2,cpmg}$ from a stretched exponential fit ($exp\left[-\left(\frac{t}{T_{2,cpmg}}\right)^{\alpha}\right]$) of the echo decay under CPMG sequence. As shown on Fig.5a, under application of CPMG dynamical decoupling pulse sequence involving N_{pulses} Pi pulses, with $N_{pulses} = 1, 2, 3, 6, 10$, we clearly observed an increase of the $T_{2,cpmg}$ spin coherence time of the shallow V2 spins (respectively, $T_{2,cpmg}$ in μs and α were found to be: (89,1.86), (111,1.79), (136,2.06), (197,1.99), (224,2.28)). To further investigate the nature of the noise filtering effect of this CPMG pulse sequence on the electronic spin bath nearby the shallow V2 spins, we plotted on Fig.5b, $T_{2,cpmg}$ as a function of N_{pulses}, the number of Pi

pulses in the CPMG sequence. We observed a saturation effect with respect to N_{pulses}, starting at a low value of N_{pulses}. This effect was previously observed for isolated shallow NV centers in diamond.[10] In this previous study on isolated shallow NV centers, the data were fitted by a function of the type $T_{2,cpmg}\left(N_{pulses}\,, N_{sat}\,, k\,, T_{2,1p}\right) = T_{2,1p}\left(N_{sat}^{k} + \left(N_{pulses}^{k} - N_{sat}^{k}\right) e^{-\frac{N_{pulses}}{N_{sat}}}\right)$. For shallow NV centers in diamond located 20 nm below the surface, the fit reported gave the parameter $k = 0.53$, close to the $k = 2/3$ expected for a simple lorentzian spin bath,[10] while for very shallow NV centers in diamond (2 or 3 nm below the surface), the fit reported gave the parameter k in the range $[0.30\,, 0.48]$.[10] Concerning the parameter N_{sat} found for shallow NV centers in diamond, it was found in the range $[13\,, 200]$,[10] depending on the depth and surface properties of the diamond surface. Here, the fit of our CPMG results at T=100K on shallow V2 spins in 4H-SiC provided the parameters: $N_{sat} = 17.38$, $k = 0.44 +/- 0.1$, $T_{2,1p} = 73360\,ns$, and thus an optimal shallow V2 spin coherence time in SiC with our CPMG noise filtering sequence of $T_{2,cpmg\infty} = 258\,\mu s$, which can be reached with a good approximation using $N_{pulses} \geq\geq N_{sat} = 17$. The value $k = 0.44 +/- 0.1$ that we found is close to the values observed for isolated shallow NV centers. This is somehow expected here because we performed CPMG experiments on V2 spins ensemble, distributed according to SRIM after C+ ion implantation, mainly between 0 nm and 25 nm below the SiC surface. This value of $k = 0.44 +/- 0.1$ is however closer to the values found for very shallow NV centers in diamond[10] which were more exposed to the surface noise, which was considered as a 2D surface spin bath with a correlation time at room temperature of around $\tau_c\left(RT\right) = 11\,\mu s$. As here, our V2 spin distribution is expected to be roughly a half gaussian with maximum at the SiC surface, this seems reasonable. This similarity in the k factor value also suggests that in our case the surface noise is also due to an electronic spin bath, as already suggested by our PELDOR experiments (Fig.3b) and Hahn echo decay experiments versus temperature (Fig.4). Note that our CPMG experiments were performed at a fixed delay $\tau = 7\,\mu s$ between the Pi pulses, corresponding to a CPMG filter function centered at around $f_0 = \frac{1}{2\tau} = 71\,kHz$. With $N_{pulses} = 10$, the spectral bandwidth of this CPMG filter is of around $7\,kHz$. Here we found a rapid saturation of $T_{2,cpmg}$ with the number of Pi pulses. This is also somehow expected because by cooling our 4H-

SiC sample at T=100K, the spin bath is also cooled and thus its correlation time becomes longer, typically on the order of the spin lattice relaxation time of the spin specy that constitute the surface spin bath at this temperature. Assuming that at 100K, the surface spin bath has a correlation time $\tau_c\,(100\,K) = 1\,ms$ (thus $f_{noise\,cutoff} = \frac{1}{\tau_c} = 1\,kHz$), with an associated spectral density of noise of the form $S(\omega) = \frac{\Delta^2}{\pi} \frac{\tau_c}{1+(\omega\,\tau_c)^2}$ (Δ being the spin qubit - spin bath coupling in this model),[10] then we see that our CPMG filter at $f_0 = \frac{1}{2\,\tau} = 71\,kHz$ with N=10 removes a large part of this noise. As the CPMG filter becomes narrower and narrower when the number of Pi pulses increase, this could explains why $T_{2,\,cpmg}$ saturates rapidly with the number of Pi pulses applied in our experimental conditions.

The remaining question is what is the fundamental decoherence process which remains in our CPMG experiments at T=100K and which is responsible for the ultimate value $T_{2,\,cpmg\,\infty} = 258\,\mu\,s$. Here we suggest two possibilities. Either, like for shallow NV centers in diamond,[10] another noise contribution has to be considered which is related to surface phonon in SiC and which would have a spectral density of noise with a frequency cutoff located at a much higher frequency, like around 10 MHz as it was found for shallow NV centers in diamond.[10] Our CPMG noise filter at $f_0 = \frac{1}{2\,\tau} = 71\,kHz$ with N=10 could thus not remove efficiently this high frequency noise, which would explain $T_{2,\,cpmg\,\infty} = 258\,\mu\,s$. The other possibility, which is possible in our study but which was not possible in the previous study of shallow NV centers, is that $T_{2,\,cpmg\,\infty} = 258\,\mu\,s$ is in fact limited by the instantaneous diffusion decoherence process[18] which exist when spin ensemble are studied and which can not be removed by CPMG dynamical decoupling methods. Thus, the ultimate spin coherence time in our sample for the shallow V2 spins would be $T_{2,\,cpmg\,\infty} = T_{ID} = 258\,\mu\,s$. To decide between those two possible explanations of $T_{2,\,cpmg\,\infty} = 258\,\mu\,s$, one needs to perform a set of similar CPMG noise spectroscopy experiments with various CPMG filter at various filter frequencies, with various bandwidth, eventually at various temperature, and on various samples with various doses of C+ ions implanted below the SiC surface. This is beyond the scope of this study and this is let for a future work.

Putting the SiC and YIG samples into contact.

To put the two 5 mm*1.8 mm SiC and YIG samples into contact, we firstly stack them horizontally on a flat clean surface. Then we also install the EPR tube horizontally and then we insert with a tweezer the stacked two samples simultaneously inside the EPR tube, at its entrance. Then we push both simultaneously at the end of the EPR tube, using another EPR tube of smaller diameter. Then, we introduce, holding the EPR tube at 45°, several small diameter quartz capillaries inside the EPR tube, allowing to fill the gap between the two solid samples stacked and the EPR tube internal wall. The last capillary is introduced in the EPR tube in a nearly vertical position and allows to introduce a small pressure on the two stacked samples placed vertically between the capillaries and the internal wall of the EPR tube.

Detailed analysis of the two shift of opposite sign observed on the V2 magnetic resonance lines when placing a YIG thin film into contact with our implanted SiC sample.

The first field direction applied was perpendicular to the normal of the two solid samples, SiC and YIG (Fig.7 top spectrum), and the second one was parallel to this normal (Fig.7 bottom spectrum). For a magnetic field applied perpendicular to the c axis of 4H-SiC, without YIG and just considering the well known spin hamiltonian $H = g\,\mu_B\,\vec{B_0}\,.\,\vec{S}\,+D\left(\vec{S}\,.\,\vec{e_c}\right)^2$, with $\vec{e_c}$ the unit vector along the C axis of 4H-SiC, $g = 2.0028$ and $D = 35\,MHz$, one expects two V2 EPR lines splited by 25 Gauss, centered around the field resonance value corresponding to $g = 2.0028$ at the fixed microwave frequency used. For a magnetic field applied parallel to the c axis of 4H-SiC, one expects, without YIG, two V2 EPR lines splittted by 50 Gauss, centered around the field resonance value corresponding to $g = 2.0028$ at the fixed microwave frequency used. We clearly observe on the Fig.7 top spectrum two V2 EPR lines splited by 25 Gauss as expected in this configuration, but not centered around a field resonance value corresponding to $g = 2.0028$ at the fixed microwave frequency used, but at a higher magnetic field value, corresponding to a shift of around $+2.5\,G$. This shift of the two EPR lines towards higher magnetic field values can be explained if one considers that a dipolar stray magnetic field produced by the YIG magnetic film is sensed by the shallow V2

spins and that it has the same direction as the one of the externally applied magnetic field, but is of opposite sens. This is qualitatively what one expects in this first experimental configuration, as schematically explained by the drawing nearby the Fig.7 top spectrum. We also clearly observe on the Fig.7 bottom spectrum two V2 EPR lines splittted by 50 Gauss as expected in this second configuration, but not centered around a field resonance value corresponding to $g = 2.0028$ at the fixed microwave frequency used, but at a lower magnetic field value, corresponding to a shift of around $-4.4\,G$. This shift of the two EPR lines towards lower magnetic field values can be explained again, if one considers that a dipolar stray magnetic field produced by the YIG magnetic film is sensed by the shallow V2 spins and that it has the same direction as the one of the externally applied magnetic field (along the c axis of SiC, which is also the <111> axis of YIG) and also the same sens. This is qualitatively what one expects in this second experimental configuration, as schematically explained by the drawing nearby the Fig.7 bottom spectrum.

One question remains which concerns the microscopic origin of this dipolar stray magnetic field sensed by the V2 spins in SiC, located below the YIG thin film, which is related to the quantitative analysis of the observed shift in the V2 magnetic resonance position. Indeed, for a uniformly magnetized thin film, with static magnetic domains of infinite dimension, one would expect no dipolar stray magnetic field which could be sensed by the V2 spins in SiC located nearby the YIG film. However, if one makes the hypothesis that we have a typical magnetic length of $60\,\mu m$ involved in this experiment (see text for discussion of its origin), then standard magnetostatic calculations (not shown) allow to explain those two shift of opposite sens, simply assuming magnetic squares (or disk) exist into the YIG thin film, with the dimension of one edge of the square being $a_{edge} = 60\,\mu m$, assuming a film thickness of $210\,nm$, and assuming a saturation magnetization of this YIG film of $B_{sat} = 1700\,G$, as confirmed by our YIG film FMR experiments (Fig.6). More precisely, the calculations show that one expect a dipolar stray magnetic field induced shift of around +2.5 G for the case where V2 spins are located anywhere within the first $6\,\mu m$ below the SiC surface and at the vertical of the center of the magnetic square considered, and when the magnetic field was applied perpendicular to the normal of the two solid samples. Calculations also show

that one expects a dipolar stray magnetic field induced shift of -5 G for the case were V2 spins are located anywhere within the first 6 μm below the SiC surface and at the vertical of the center of the magnetic square considered, and when the magnetic field was applied parallel to the normal of the two solid samples. The magnetostatic calculations are thus in good quantitative agreement with the experimentally observed shift.

References

(1) M. Widmann et al., Nature Materials **14**, 164 (2015).

(2) D. Simin et al., Phys. Rev. B **95**, 161201(R) (2017).

(3) J.S. Embley et al., Phys. Rev. B **95**, 45206 (2017).

(4) J. Tribollet, Eur. Phys. J. Appl. Phys. 90, 20103 (2020).

(5) R. Nagy et al., Nature Comm. **10**, 1954 (2019)

(6) H.B. Banks, Phys. Rev. Applied 11, 24013 (2019).

(7) J. Tribollet, Eur. Phys. J. Appl. Phys. 90, 20102 (2020).

(8) J. Tribollet et al., Eur. Phys. J. B. **87**, 183 (2014).

(9) S. Castelleto et al., J. Phys. Photonics **2**, 022001 (2020).

(10) Y. Romach et al., Phys. Rev. Letters **114**, 17601 (2015).

(11) J. Wang et al., Phys. Rev. Applied **7**, 64021 (2017).

(12) J. Wang et al., ACS Photonics **4**, 1054 (2017).

(13) Q. Li et al., Nanoscale **11**, 20544 (2019).

(14) S. Agnello et al., Phys. Rev. A **59**, 4087 (1999).

(15) R.N. Shakhmuratov et al., Phys. Rev. Letters **79**, 2963 (1997).

(16) J.F. Ziegler et al., Nuclear Instruments and Methods in Physics Research section B Beam interaction with Materials and Atoms **268**, 1818 (2010).

(17) G. de Lange et al., Science **330**, 60 (2010).

(18) A. Schweiger et al., Principles of pulse electron paramagnetic resonance, Oxford University Press, Oxford UK; New York (2001).

(19) D.P. DiVincenzo, Fortschr. Phys. **48**, 771 (2000).

(20) P. Pirro et al., Appl. Phys. Lett. **104**, 12402 (2014).

(21) J. Wang et al., ACS Photonics **6**, 1736 (2019).

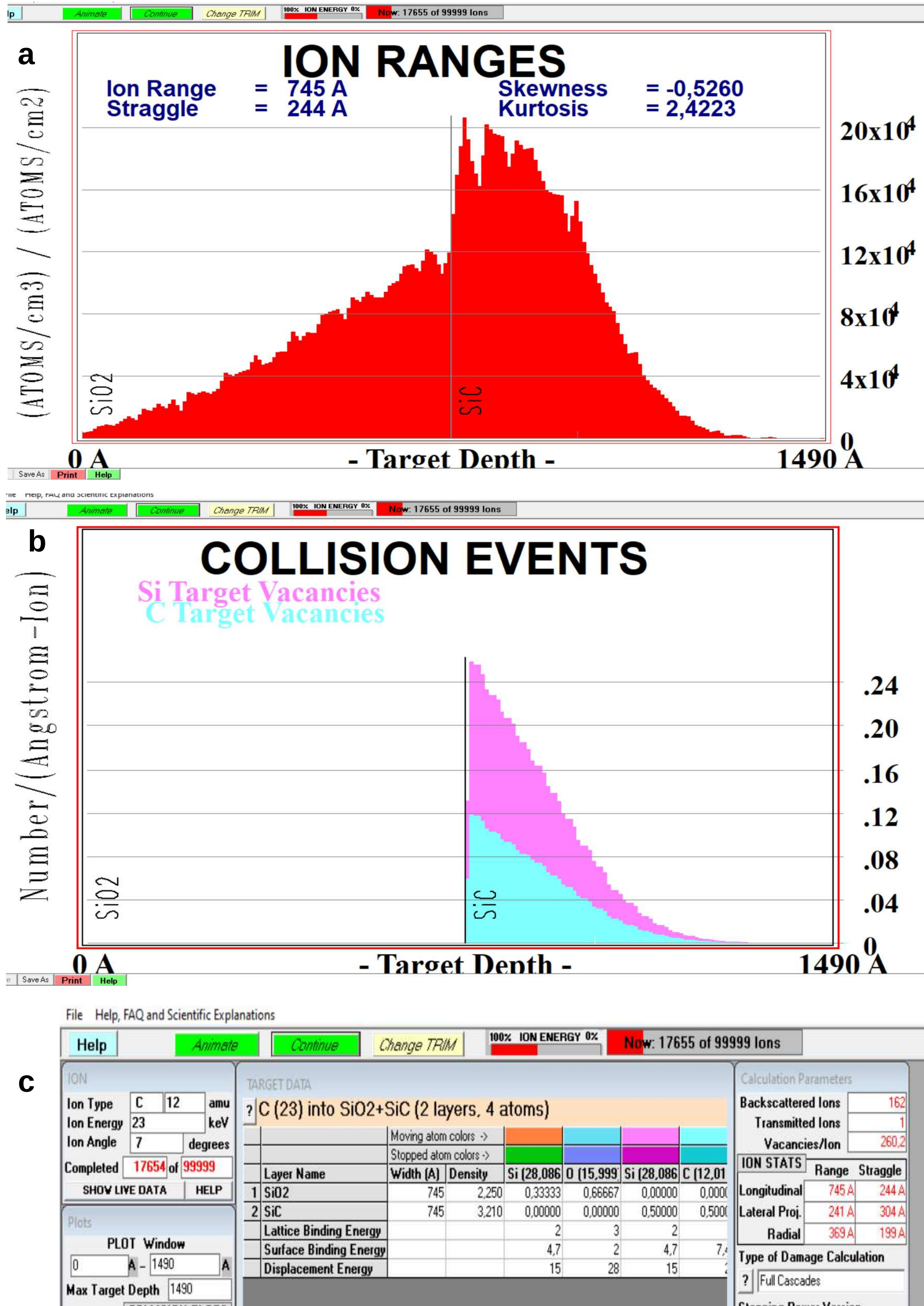

Figure 1: This figure 1 is called Fig.8 in the above text of ESI. SRIM simulation of the ion implantation process of 23 keV C+ ions through a 74.5 nm SiO2 sacrificial layer present on top of the 4H-SiC substrate pre-processed (see text).

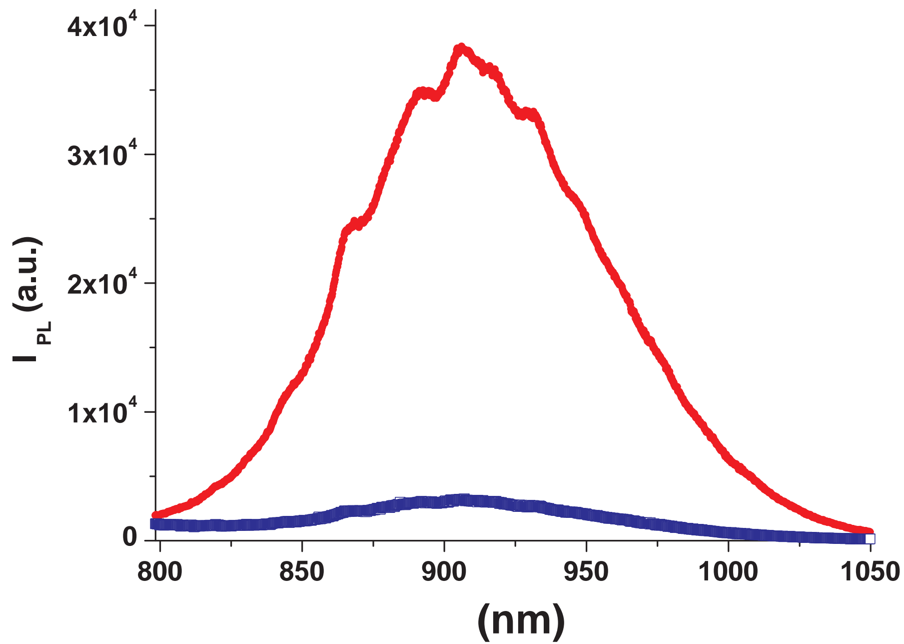

Figure 2: This figure 2 is called Fig.9 in the above text of ESI. Infrared micro-photoluminescence spectrum of the 8 days annealed 4H-SiC reference sample (in blue) and the one of the fully processed and ion implanted 4H-SiC sample studied here in details (in red). Spectrum obtained on a micro-Raman spectrometer at RT (300K), objective *100, NA=0.9, Plaser= 90mW at 532 nm, Tinteg= 60sec.